Journal of the European Ceramic Society 20 (2000) 463–472

Deformation and damage processes during tensile creep of ceramic-fibre-reinforced ceramic–matrix composites

B. Wilshire*, F. Carreño[1]

Department of Materials Engineering, University of Wales, Swansea SA2 8PP, UK

Received 10 May 1999; received in revised form 21 June 1999; accepted 28 June 1999

Abstract

The tensile creep and creep fracture properties in air at 1300°C are compared for SiC_f/SiC and SiC_f/Al_2O_3 composites, each reinforced with 0.38 volume fractions of interwoven silicon carbide (Nicalon™) fibre bundles aligned parallel and normal to the stress direction. The differing behaviour patterns displayed by these 0/90° woven composites are analysed to identify the processes controlling creep strain accumulation and crack development.

Keywords: Composites; Creep; Fracture; SiC_f/Al_2O_3; SiC_f/SiC

1. Introduction

For service applications involving creep loading at high temperatures, continuous ceramic-fibre-reinforced ceramic–matrix composites (CFCCs) offer the prospect of combining high strength, good oxidation resistance and low density, while avoiding the engineering design constraints imposed by the inherently brittle nature of monolithic ceramics. With this class of materials, the strength characteristics depend primarily on load transfer to large volume fractions of high-modulus fibres with weak fibre/matrix interfaces.[1–3] Yet, while several studies have provided insights into the mechanisms controlling creep of these fibre-reinforced composites,[4–12] few comparisons have been made of the relative creep strengths of different CFCCs.[8] For this reason, the tensile creep and creep fracture properties in air at 1300°C have been compared for two high-performance CFCCs; one with a silicon carbide matrix and the other with an alumina matrix, both reinforced with interwoven bundles of silicon carbide (Nicalon™) fibres oriented parallel and normal to the stress axis. The data comparisons were supported by microstructural studies and by creep curve shape analyses, allowing all features of the behaviour patterns exhibited by these 0/90° woven CFCCs to be rationalized in terms of the processes shown to govern creep strain accumulation and rupture ductility.

2. Experimental procedures

The silicon carbide fibre-reinforced silicon carbide (SiC_f/SiC) had a plain weave Nicalon™ fibre arrangement, with a fibre volume fraction of ~0.38.[12] To provide the weak interface layers, carbon (< 0.5 μm thick) was deposited on the ~15 μm diameter Nicalon™ NLM202 fibres before the fibre preforms were densified by chemical vapour infiltration (CVI) to form the polycrystalline SiC matrix, which had a total porosity of ~15% [Fig. 1(a)].

CFCCs can be produced with more complex structures, as exemplified by a Nicalon™ fibre-reinforced alumina-matrix (SiC_f/Al_2O_3) composite developed by Dupont Lanxide Composites Inc. (now Allied Signal). With this material, eight-harness satin-woven Nicalon™ NLM202 fibres were coated with boron nitride, which formed the thin interface layers between the ~15 μm diameter fibres and the CVI-deposited SiC fibre coatings (~5 μm thick). The alumina matrix was then introduced via the DIMOX process, i.e. by in-situ directional oxidation of liquid aluminium.[13,14] A subsequent metal removal operation reduced the residual metal content to < 4%, creating a polycrystalline alumina

* Corresponding author. Tel.: +44-(0)1792-295-243; fax: +44-(0)1792-295-244.

E-mail address: b.wilshire@swansea.ac.uk (B. Wilshire).

[1] Present address: Centro Nacional de Investigaciones Metalúrgicas, CSIC, 28040 Madrid, Spain.

0955-2219/00/$ - see front matter
PII: S0955-2219(99)00175-2

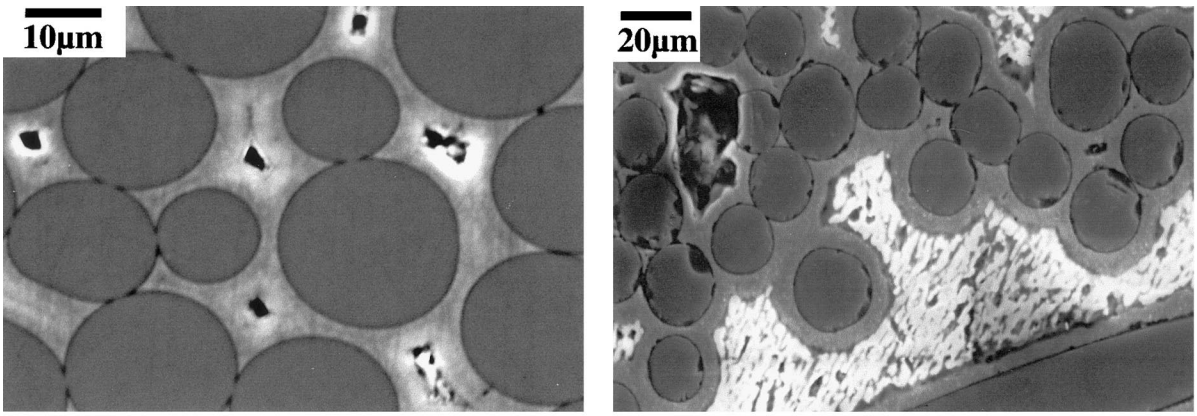

Fig. 1. Scanning electron micrographs showing (a) the carbon-coated Nicalon™ fibres in the silicon carbide matrix of the SiC_f/SiC composite and (b) the double BN/SiC coated Nicalon™ fibres in the alumina matrix of SiC_f/Al_2O_3 composite.

matrix with a porosity less than 15% [Fig. 1(b)]. This results in a matrix modulus substantially lower than that of the coated fibre tows.

For both types of CFCC, the 2D layers of woven fabric or plies were aligned and stacked before densification, resulting in multi-layer samples with fibre bundles arranged into balanced 0/90° woven arrays. However, certain distinctive features of the composite structures should be noted. Although both CFCCs contained ~0.38 volume fractions of ~15 μm diameter Nicalon™ NLM202 fibres, the weave patterns were different, with the fibre bundle configurations illustrated in Figs. 2 and 3. In addition to differing matrix compositions, the SiC_f/SiC material had thin carbon interfaces between the fibres and the matrix, whereas the SiC_f/Al_2O_3 composite was produced with the fibres having double BN/SiC coatings. Furthermore, while pores (~1 to 20 μm diameter) were readily apparent within the fibre bundles of both composites (Fig. 1), only with the SiC_f/SiC samples were macropores (up to several 100 μm in length) routinely found in the matrix regions between the interwoven fibre bundles [Figs. 2 and 3].

To ensure that valid comparisons could be made between the data sets obtained for both CFCCs, the procedures adopted to evaluate the SiC_f/SiC composite[12] were also used for the SiC_f/Al_2O_3 material. Thus, tensile creep tests were carried out using samples produced such that stresses were applied parallel to one fibre direction. The flat 200 mm long specimens had gauge lengths of 40 mm and widths of 8 mm, with the testpiece thicknesses being 2.8 mm for the SiC_f/Al_2O_3 compared with 3.5 mm for the SiC_f/SiC composite. The tests were conducted in air at 1300°C, using high-precision machines described elsewhere.[12,15] In all cases, loading was performed once the specimens had stabilized for 1 h at the test temperature, with the loads applied smoothly

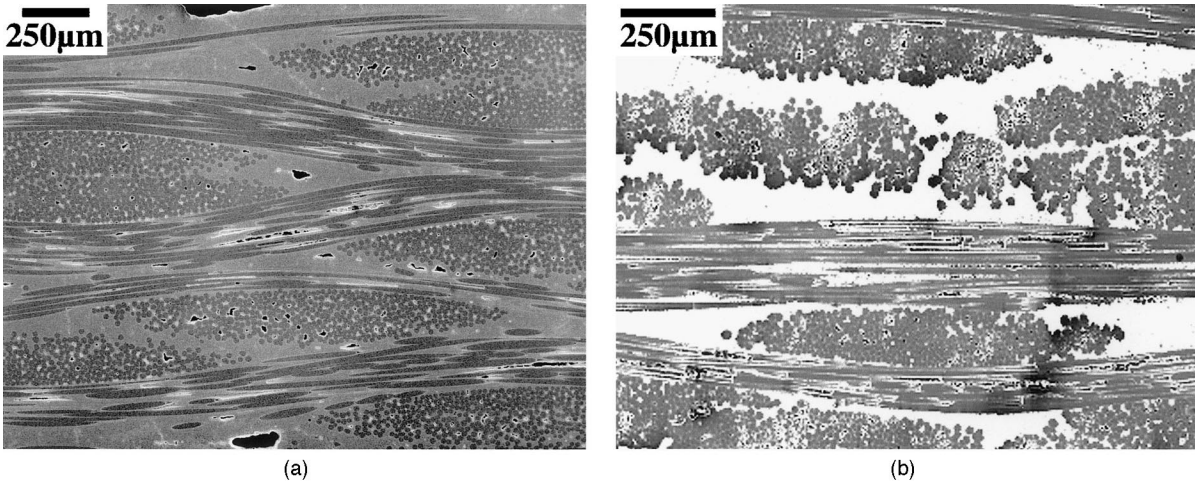

Fig. 2. Scanning electron micrographs showing the through-thickness appearances of the fibre bundles in the as-received (a) SiC_f/SiC and (b) SiC_f/Al_2O_3 composites. In relation to these bundle configurations, the tensile stress axis would be horizontal. For clarity, some of the macropores between the interwoven fibre bundles in the SiC_f/SiC material have been infilled black.

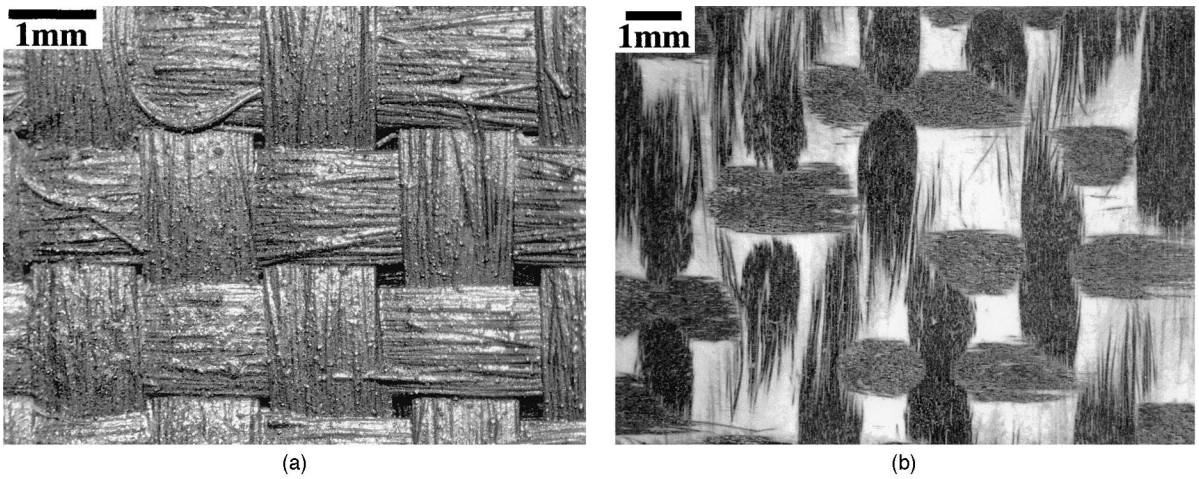

Fig. 3. The appearances of (a) the un-ground surfaces of the SiC_f/SiC specimens and (b) the ground surfaces of the SiC_f/Al_2O_3 testpieces.

by means of a slow-release jack. Yet, while stresses from 47 to 80 MPa were chosen for the study of the SiC_f/SiC samples,[12] stresses from 60 to 95 MPa were required to give creep lives up to around 2500 h with the SiC_f/Al_2O_3 specimens.

Few problems were encountered in testing the SiC_f/Al_2O_3 samples, which were surface ground prior to creep exposure to give a maximum of seven undamaged woven layers or plies across the testpiece thickness. With the unground SiC_f/SiC specimens, problems were sometimes caused by failure outside the testpiece gauge length and occasionally by slippage from the grips.[12] Only results free from these experimental difficulties were included in the present analysis.

3. Results and discussion

As found for the SiC_f/SiC composite tested in air at 1300°C,[12] at each stress level investigated for the SiC_f/Al_2O_3 material, after the initial strain on loading at the creep temperature, a normal primary curve was observed during which the creep rate decreased with time to a minimum value. Over the stress ranges considered, no well-defined secondary or tertiary stages were apparent, although very short periods of rapid creep rate acceleration became more evident just prior to fracture at low stresses (Fig. 4). However, with the SiC_f/Al_2O_3 samples, the strain to failure increased with decreasing stress, resulting in creep ductilities substantially greater than those recorded for the SiC_f/SiC material,[12] particularly in tests of long duration (Fig. 5).

3.1. Factors affecting creep strength

For each creep curve obtained for the SiC_f/Al_2O_3 composite, the value of the minimum rate was determined, allowing comparisons to be made with tensile creep data acquired at 1300°C for

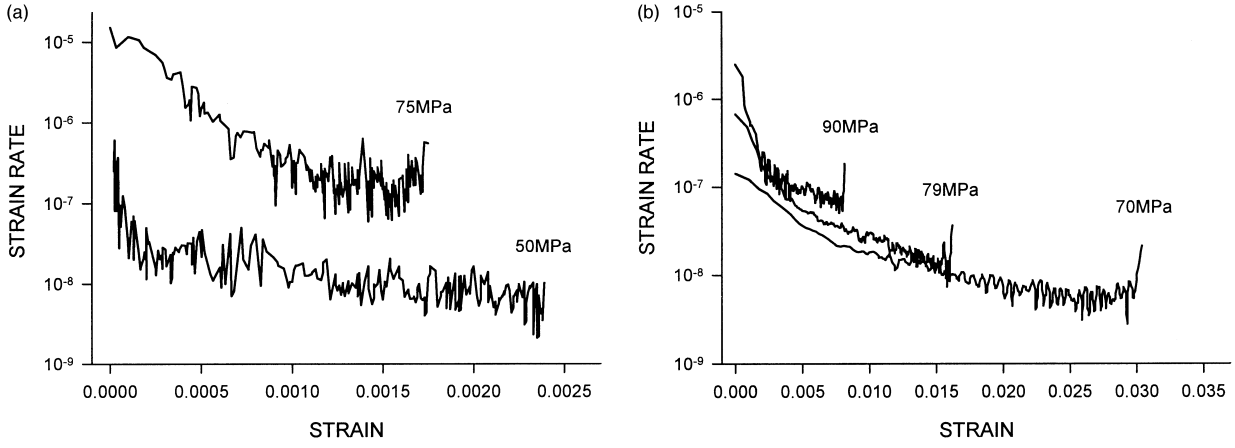

Fig. 4. Tensile creep curves for (a) the SiC_f/SiC and (b) the SiC_f/Al_2O_3 composites in air at 1300°C, plotted as creep rate against creep strain at various stress levels.

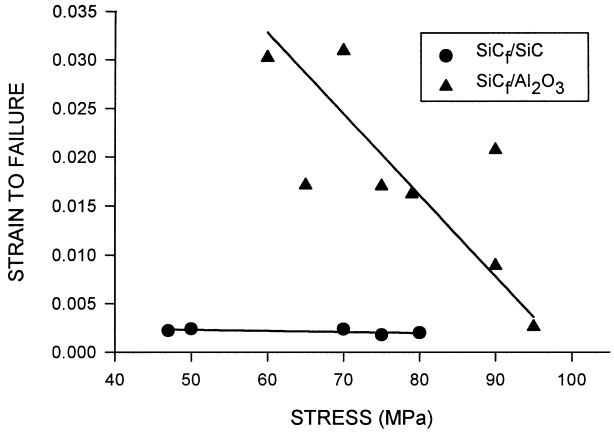

Fig. 5. The stress dependence of the creep strain to failure in air at 1300°C for the SiC_f/SiC and SiC_f/Al_2O_3 composites.

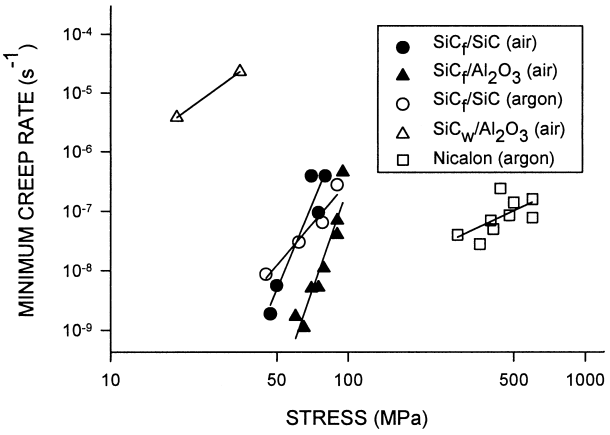

Fig. 6. The variations of the minimum creep rate with stress at 1300°C for the SiC_f/Al_2O_3 composite, with tensile creep data included for 0/90° woven SiC_f/SiC materials,[10,12] for a SiC_w/Al_2O_3 ceramic[16] and for Nicalon™ NLM202 fibres.[17]

a. the SiC_f/SiC samples in air,[12]
b. a 25 vol% SiC whisker-reinforced alumina–matrix ceramic (SiC_w/Al_2O_3) in air[16] and
c. Nicalon™ NLM202 fibres under vacuum.[17]

It has been suggested recently that creep of the matrix governs the creep properties displayed by 0/90° woven SiC_f/SiC materials.[18] This conclusion was based on the observation that matrix cracking was not excessive. Moreover, the creep rates reported for silicon carbide produced by chemical vapour deposition[19] appeared to be lower than those derived by extended extrapolation of results obtained for Nicalon™ fibres.[17] Although the present study confirms the low incidence of large cracks even at fracture of the SiC_f/SiC samples, several observations demonstrate that the Nicalon™ fibres control the rates of creep strain accumulation in both the SiC_f/SiC and SiC_f/Al_2O_3 composites, with creep of the fibres accompanied by matrix microcracking.

From Fig. 6, it is clear that stresses about five times higher must be applied to the Nicalon™ fibres in order to achieve creep rates comparable with those recorded for the Nicalon™ fibre-reinforced materials. The creep performance of the SiC_f/SiC and SiC_f/Al_2O_3 products must therefore be governed by the longitudinal fibres, which occupy approximately one fifth of the testpiece cross-section.

The dominant rôle of the fibres was confirmed by data comparisons for the SiC_w/Al_2O_3 and SiC_f/Al_2O_3 composites in air at 1300°C. The incorporation of SiC whisker dispersions improves the creep strength of fully-dense alumina,[20–22] but the creep resistance of the fibre-reinforced alumina is considerably greater than that of the whisker-reinforced ceramic (Fig. 6). Consequently, the porous alumina matrix can make little contribution to the creep strength of the SiC_f/Al_2O_3 composite.

Since the fibres determine the creep strength, similar property values could be expected for tests carried out in air at 1300°C for the SiC_f/SiC and SiC_f/Al_2O_3 samples, which both contained 0.38 volume fractions of ~15 μm diameter Nicalon™ fibres arranged as 0/90° woven arrays. Yet, the minimum rates recorded for the SiC_f/Al_2O_3 composite were more than an order of magnitude lower than those for the SiC_f/SiC product over comparable stress ranges (Fig. 6). In addition to this superior creep resistance, the stress rupture data in Fig. 7 reveal that the times to fracture were over 100 times longer for the SiC_f/Al_2O_3 samples than for the SiC_f/SiC testpieces under equivalent test conditions.

These seemingly anomalous results can be explained by considering the detailed shapes of the creep strain/time curves. Fig. 8 shows the curves recorded at the same applied stress for the SiC_f/Al_2O_3 and SiC_f/SiC composites. Compared with the large differences in creep and stress rupture resistance noted in Figs. 6 and 7, the initial creep rates were only about 4 times faster for the SiC_f/SiC specimens over similar stress ranges

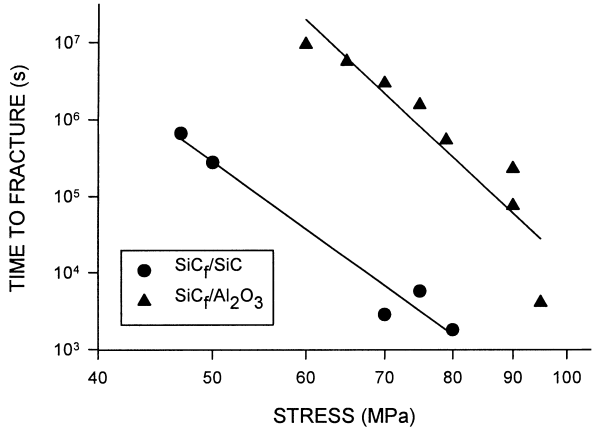

Fig. 7. The variations of the creep rupture life with stress in air at 1300°C for the SiC_f/SiC and SiC_f/Al_2O_3 composites.

(Fig. 8), which may be attributable to differences in the fibre coating types and weave patterns and/or to the presence of macroporosity (Figs. 1–3). Even so, these differences in initial creep strength become exaggerated because, when continuously-decaying curves are recorded (Figs. 4 and 8), the minimum creep rates and rupture lives are influenced by variations in the strain to failure (Fig. 5).

Under uniaxial tension, the rupture life (t_f) can be defined as the time (t) taken for the accumulated creep strain (ε) to reach the limiting creep ductility (ε_f). Thus, continuously decaying curves of the form shown in Figs. 4 and 8 can be considered to terminate at $t = t_f$ when $\varepsilon = \varepsilon_f$, with the creep rate ($\dot{\varepsilon}$) decreasing gradually from an initial high value until a minimum rate ($\dot{\varepsilon}_m$) is attained essentially at the point of failure. On this basis, since the strains to failure are low for the SiC_f/SiC material at all stress levels (Fig. 5), the creep curves terminate early (Fig. 8), giving high minimum creep rates and low rupture lives (Figs. 6 and 7). In contrast, particularly in longer term tests with the SiC_f/Al_2O_3 product, the creep rate decays continuously until fracture occurs at relatively high strains (Figs. 5 and 8), resulting in lower minimum rates and much longer times to fracture (Figs. 6 and 7). Hence, to interpret the varying behaviour patterns exhibited by these 0/90° woven CFCCs, it is necessary to identify the damage processes determining the creep ductilities (Fig. 5).

3.2. Creep fracture processes

The damage processes leading to failure were clarified by microstructural examination and fractographic studies, extending the preliminary investigation carried out for the SiC_f/SiC composite[12] to allow comparisons to be made with the crack development patterns observed in air at 1300°C for the SiC_f/Al_2O_3 composite.

With both materials, creep of the longitudinal Nicalon™ fibres was accompanied by cracking of the weak brittle matrices. The cracks could grow through the transverse bundles, by-passing the fibres (Fig. 9), also crossing the fibre-free matrix regions between the individual layers of woven fabric before becoming arrested by the longitudinal fibre bundles (Fig. 10). On penetrating into the longitudinal bundles in a direction normal to the stress direction, the cracks became bridged by the fibres,[1–3] but the bridging fibres then failed progressively as oxygen penetrated during tests in air.[23] This resulted in cracks developing with oxidation-assisted fibre failure occurring essentially in the fracture plane (Fig. 11). For both CFCCs, crack growth zones with in-plane fibre failure were therefore observed, together with regions where sudden fracture occurred by fibre pull-out (Fig. 12), although the detailed appearances of the fracture surfaces differed for the SiC_f/SiC and SiC_f/Al_2O_3 composites.

With the SiC_f/SiC testpieces, a zone showing fibre pull-out of the longitudinal bundles was observed only in one region of the fracture surface, with this zone surrounded by the region of near-planar crack development with negligible pull-out [Fig. 12(a)]. The percentage of

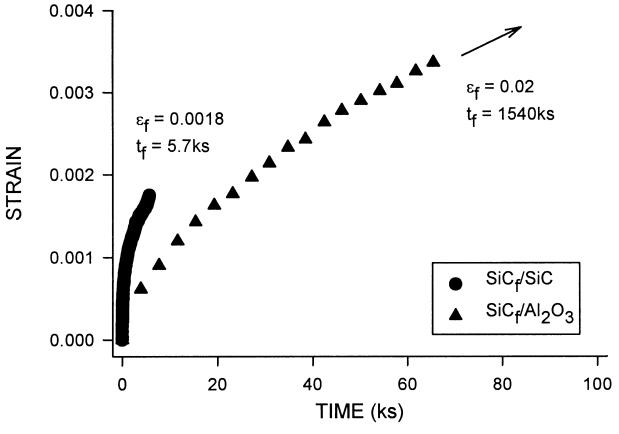

Fig. 8. Creep strain/time curves for the SiC_f/SiC and SiC_f/Al_2O_3 composites tested in air at 1300°C under a stress of 75 MPa.

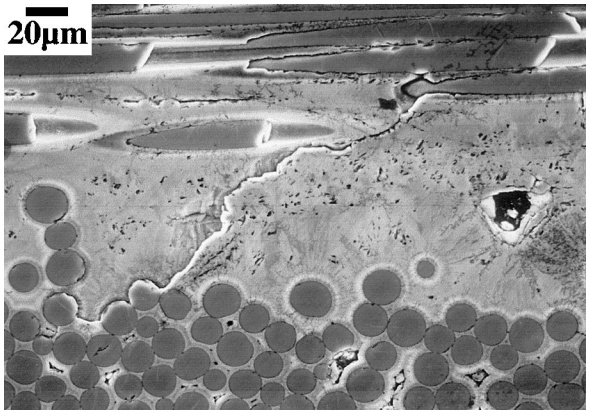

Fig. 9. Scanning electron micrograph showing matrix crack development in the SiC_f/SiC composite tested in air at 1300°C.

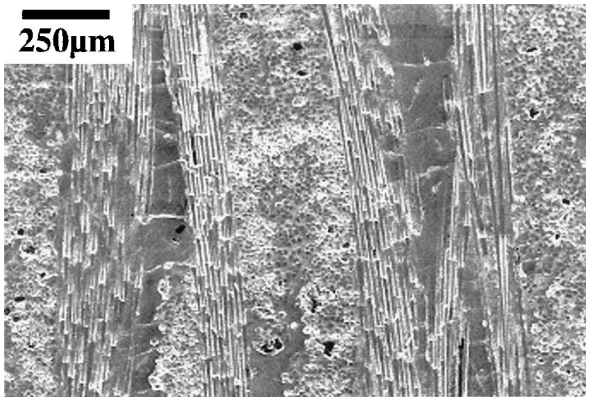

Fig. 10. Scanning electron micrograph showing cracks penetrating across the matrix regions between the interwoven layers of fabric in the SiC_f/Al_2O_3 composite. The tensile stress axis is vertical.

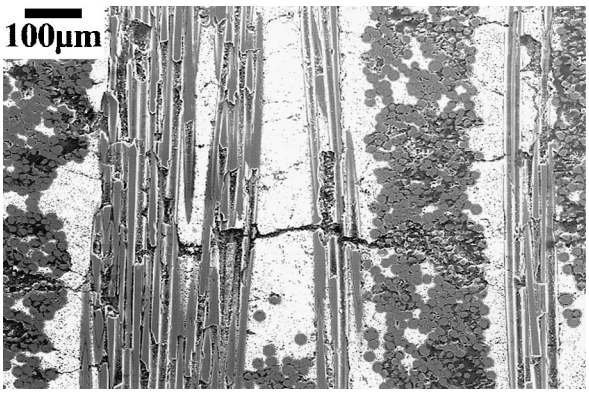

Fig. 11. Scanning electron micrograph showing crack penetration through a longitudinal fibre bundle in the SiC_f/Al_2O_3 composite. The tensile stress axis is vertical.

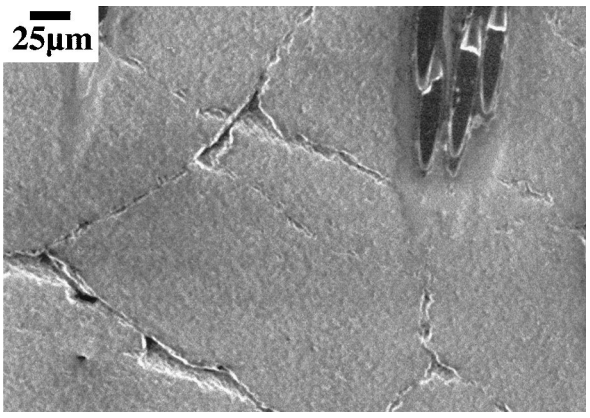

Fig. 13. Scanning electron micrograph showing extensive crack development in the matrix of the SiC_f/Al_2O_3 composite during creep in air at 1300°C.

the final testpiece cross-section occupied by the near-planar crack increased from ~25 to ~75% with decreasing stress, suggesting that fracture occurred when a dominant crack grew to the size required to cause sudden failure by fibre pull-out. This conclusion is consistent with the fact that, away from the fracture surfaces, large cracks were rarely discernible along the gauge lengths of the SiC_f/SiC testpieces.

Cracks developed more uniformly throughout the SiC_f/Al_2O_3 samples (Fig. 10), indicating that crack growth and link up caused failure when the total area of near-planar cracks reached a critical fraction of the cross-sectional area. As a result, fibre pull-out occurred in a number of non-connected zones distributed across the fracture surfaces [Fig. 12(b)], but with the fractional area of the near-planar cracks at fracture varying only from ~60 to ~80% over the entire stress range studied.

These differences in the crack development pattern (Fig. 12) can be rationalized in the following manner. In the as-processed state, the SiC_f/Al_2O_3 samples contain residual stress-induced micro-cracks,[24] which facilitate crack formation in the alumina matrix as the creep strain accumulates (Fig. 13). Yet, while cracks form extensively throughout the SiC_f/Al_2O_3 testpieces (Fig. 10), nucleation occurs preferentially where high stress concentrations arise at macropores present in the matrix regions between the interwoven fibre bundles in the SiC_f/SiC material (Figs. 2 and 3). Individual cracks were often observed to originate at these macropores [Fig. 14(a)] and to connect between neighbouring macropores [Fig. 14(b)]. Once link up takes place between cracks nucleated at several macropores, the resulting large crack grows rapidly through the longitudinal bundles by oxidation-assisted failure of the bridging fibres, causing fracture before other large cracks develop. In addition to demonstrating the existence of favourable crack nucleation sites, these observations suggest that crack growth rates are significantly faster in the SiC_f/SiC specimens.

3.3. Factors affecting crack growth rates

The rôle of oxidation-assisted fibre failure in relation to crack growth rates was investigated by reference to the creep-rate dependences of the rupture lives. For the SiC_f/SiC and SiC_f/Al_2O_3 composites, the time to fracture

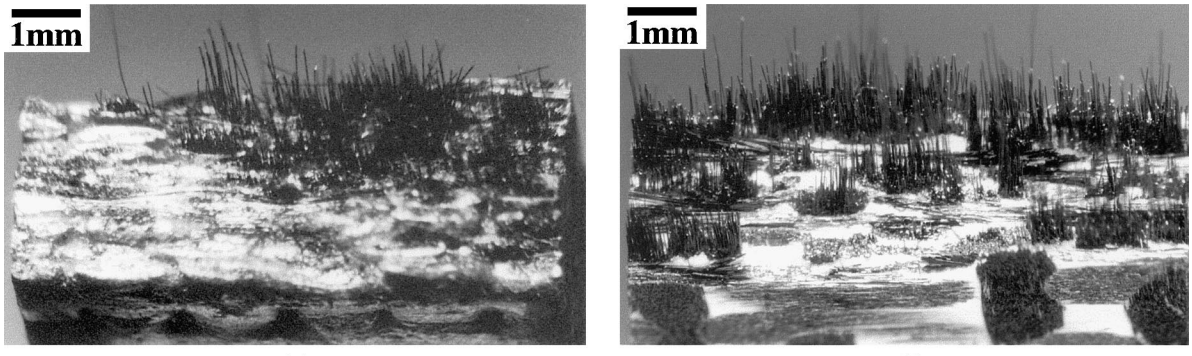

Fig. 12. Scanning electron micrographs showing the crack-growth zones characterized by in-plane fibre failure and the final fibre pull-out zones on the creep fracture surfaces of (a) the SiC_f/SiC and (b) the SiC_f/Al_2O_3 composites crept to failure in air under a tensile stress of 75 MPa at 1300°C.

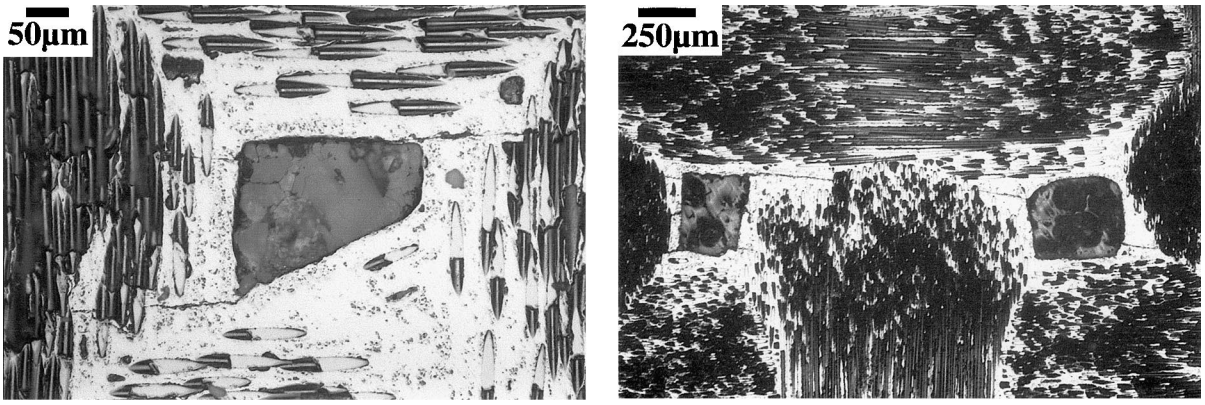

Fig. 14. Scanning electron micrographs showing (a) cracks developing from a macropore and (b) link up of cracks nucleating at adjacent macropores during creep of the SiC_f/SiC composite in air at 1300°C.

decreased with increasing minimum creep rate (Fig. 15), showing that fracture is strain controlled.

The rupture lives represent the total times taken for cracks to grow completely through many longitudinal fibre bundles, in order to attain the areas of near-planar cracking required to cause failure by fibre pull-out (Fig. 12). The dependences of t_f on $\dot{\varepsilon}_m$ (Fig. 15) can then be explained on the basis that the longitudinal fibre bundles govern the rates of creep strain accumulation, with the crack-bridging fibres then determining the rates of crack growth through the longitudinal bundles. Even so, fibre failure is accelerated by oxidation.

The ways in which variables such as fibre diameter and fibre-coating types affect oxidation-assisted fibre failure and crack growth can be explored by comparing the $\dot{\varepsilon}_m/t_f$ data in Fig. 15

a. for two types of SiC_f/SiC composite tested in air[12] and argon[10] and
b. for the SiC_f/Al_2O_3 material tested in air.

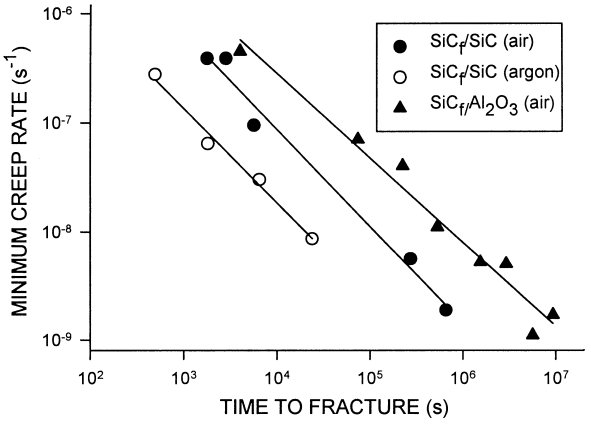

Fig. 15. The relationships between the minimum creep rates and the creep rupture lives at 1300°C for the SiC_f/Al_2O_3 material in air and for SiC_f/SiC composites in argon[10] and air.[12]

The 0/90° woven SiC_f/SiC composites were both reinforced with 0.38 volume fractions of carbon-coated Nicalon™ NLM202 fibres, but the fibre diameter was quoted as ~12 μm for the samples tested in argon[10] compared with ~15 μm for the specimens tested in air[12] [Fig. 1(a)]. These materials showed similar creep strengths over comparable stress ranges at 1300°C, as evident from Fig. 6. Moreover, the appearances of the fracture surfaces for SiC_f/SiC samples crept to failure under argon[10] were identical to those shown in Fig. 12(a) for tests in air,[12] in line with the observation that even low partial pressures of oxygen in the test atmospheres accelerate fibre failure and crack growth rates.[8] Even so, for a fixed creep rate, the rupture life in argon[10] was almost an order of magnitude lower than the time to fracture recorded for the SiC_f/SiC composite tested in air.[12] Since oxidation rates must be higher in air than under the low oxygen partial pressures encountered in argon atmospheres, this evidence indicates that the rates of oxidation-assisted fibre failure and crack growth increase with decreasing fibre diameter.

The results in Fig. 15 also show that, for a fixed creep rate in air at 1300°C, the rupture life of the SiC_f/SiC samples was about an order of magnitude lower than that for the SiC_f/Al_2O_3 specimens, even though both CFCCs had comparable fibre types, volume fractions and architectures (Figs. 1–3). For the same rate of creep strain accumulation, shorter rupture lives are a consequence of higher crack growth rates through the longitudinal fibre bundles, suggesting that the carbon-coated fibres in the SiC_f/SiC composite are more prone to oxidation-assisted failure than the double BN/SiC coated fibres in the SiC_f/Al_2O_3 material. However, variations in crack growth rates may also be attributable to differences in the ways in which oxygen from the test atmosphere reaches the bridging fibres.

It would seem reasonable to assume that oxygen penetrates inward from the specimen surfaces, but this

should lead to the near-planar cracks developing until fracture occurs with a fibre pull-out zone near the centre of the testpiece. Yet, with the SiC_f/SiC samples, the pull-out zone was often located at a near-surface position [Fig. 12(a)], suggesting that the dominant crack nucleates at or near one surface of the specimen. The large crack opening displacements associated with a growing surface crack would then allow direct oxygen penetration, promoting fibre failure in the crack plane. In this way, the dominant crack would grow rapidly until the remaining unbroken fibre bundles are unable to carry the load, resulting in a pull-out zone in one region which may or may not be located centrally on the fracture surface [Fig. 12(a)].

With the SiC_f/Al_2O_3 material, failure occurred by growth and link up of several separately-nucleated cracks, but even the near-planar cracks formed towards the centres of the specimens were devoid of fibre pull-out [Fig. 12(b)]. Oxidation-assisted fibre failure at cracks unconnected to the surface may then be associated with general oxygen penetration into the testpieces through the residual stress-induced matrix microcracks present before loading[24] and certainly after loading (Fig. 13). Compared with direct oxygen penetration along a dominant crack in the SiC_f/SiC material, indirect oxygen ingress could be a significant factor contributing to the lower rates of crack growth in the SiC_f/Al_2O_3 composite.

The crack growth rates, as well as the patterns of crack formation, determine the creep strains to failure. With both CFCCs, the near-planar crack area/cross section ratio at fracture increased with decreasing stress. The low growth rates of cracks forming throughout the SiC_f/Al_2O_3 testpieces therefore defer fracture to longer times and higher strains so that, since larger crack areas must develop to cause failure as the test duration increases, the creep ductility increases with decreasing stress (Fig. 5). In contrast, the rapid growth of a dominant crack results in low-ductility failure at all stresses studied for the SiC_f/SiC composite.

3.4. Analysis of creep curve shapes

Ductility variations (Fig. 5) influence the measured values of the minimum creep rate (Fig. 6) and rupture life (Fig. 7), as evident from qualitative inspection of the creep strain/time curves shown in Fig. 8. Yet, quantitative analyses of creep curve shapes are necessary to explain why, for both 0/90° woven CFCCs, the stress dependences of the creep ductility (Fig. 5) determine the stress dependences of the product, $\dot{\varepsilon}_m.t_f$ (Fig. 16), such that

$$\dot{\varepsilon}_m t_f = X\varepsilon_f \tag{1}$$

with X being a constant ($\cong$0.5) at 1300°C.

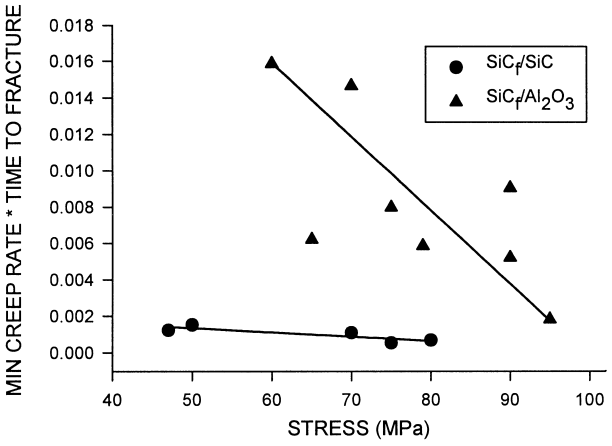

Fig. 16. The variations of the product ($\dot{\varepsilon}_m.t_f$) of the minimum creep rate and the creep rupture life with stress in air at 1300°C for the SiC_f/SiC and SiC_f/Al_2O_3 composites.

A variety of different expressions have been devised to describe the shapes of decaying creep curves,[25] one option being that the creep strain varies with time as

$$\varepsilon = at^x \tag{2}$$

where a and x are constants, accounting for Eq. (1) when $x = X \cong 0.5$. However, this equation predicts an infinite initial creep rate and a creep rate which decays continuously without ever reaching a steady value. To avoid these limitations, decaying curves are often described as[26,27]

$$\varepsilon = \theta_1[1 - \exp(-\theta_2 t)] + \theta_3\theta_4 t \tag{3}$$

where θ_1 scales the primary stage with respect to strain, the rate parameter θ_2 governs the curvature of the primary stage and $\theta_3\theta_4 = \dot{\varepsilon}_m$. For each curve obtained for the SiC_f/SiC and SiC_f/Al_2O_3 composites, the best values of θ_1, θ_2 and $\theta_3.\theta_4$ were computed using a least-squares curve-fitting routine,[28] with a reasonable description of individual curves being obtained by substitution of the derived θ values into Eq. (3). During each test, the creep rate therefore decreases with time as

$$\dot{\varepsilon} = \theta_1\theta_2 \exp(-\theta_2 t) + \dot{\varepsilon}_m \tag{4}$$

reaching the minimum value when the primary component becomes negligible. This occurs as $t \to t_f$, when

$$\theta_2 t_f = Y \tag{5}$$

where $Y \cong 4$ (Fig. 17). From Eq. (3), at fracture,

$$\varepsilon_f = \theta_1 + \dot{\varepsilon}_m t_f \tag{6}$$

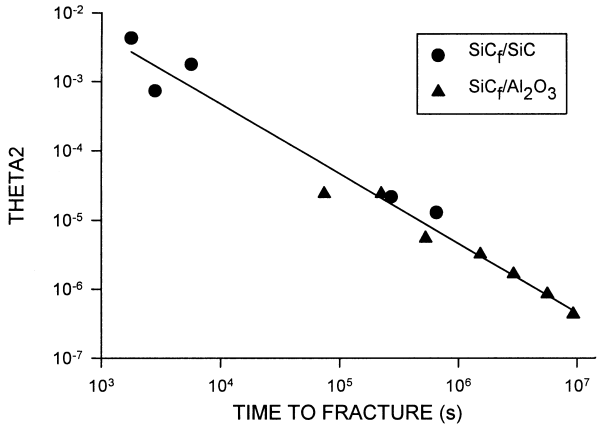

Fig. 17. The dependence of the creep rupture life on the primary rate parameter, θ_2, for the SiC_f/SiC and SiC_f/Al_2O_3 composites in air at 1300°C.

Moreover, from Eq. (4), the initial creep rate ($\dot{\varepsilon}_o$) at $t = 0$ can be computed as

$$\dot{\varepsilon}_0 = \theta_1\theta_2 + \theta_3\theta_4 = \theta_1\theta_2 + \dot{\varepsilon}_m \tag{7}$$

As reported for both metallic and ceramic materials,[29,30] the computed initial rate is discernibly lower than the measured initial rate determined directly from the experimental creep curve, because the creep rate decays very rapidly immediately after the initial strain on loading. Even so, the results in Fig. 18 make it clear that $\dot{\varepsilon}_o \propto \dot{\varepsilon}_m$, with

$$\dot{\varepsilon}_m = Z(\dot{\varepsilon}_o - \dot{\varepsilon}_m) \tag{8}$$

where $Z \cong 0.25$. Combining Eqs. (5), (6) and (8) then gives

$$\dot{\varepsilon}_m t_f/\varepsilon_f = X = [YZ/(1 + YZ)] \tag{9}$$

with $YZ \cong 1$, so that $X \cong 0.5$, in line with Eq. (1).

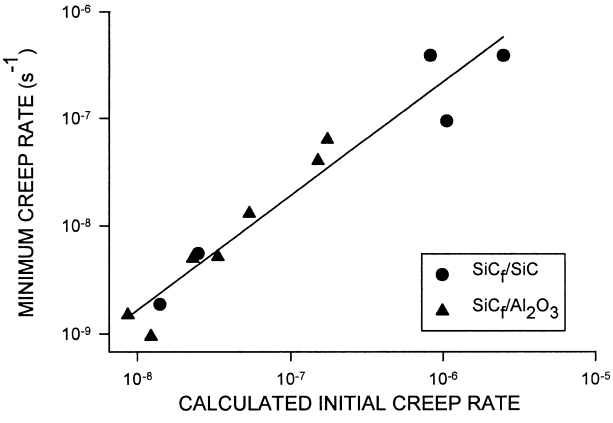

Fig. 18. The relationship between the computed initial creep rate ($\dot{\varepsilon}_o$) and the measured minimum creep rate ($\dot{\varepsilon}_m$) for the SiC_f/SiC and SiC_f/Al_2O_3 in air at 1300°C.

While Eqs. (2) and (3) provide satisfactory descriptions of the seemingly-smooth ε/t curves recorded for the present CFCCs (Fig. 8), the serrated appearances of the $\dot{\varepsilon}/\varepsilon$ curves (Fig. 4) suggest that the creep strain accumulates in 'mini-bursts', especially as $\dot{\varepsilon} \to \dot{\varepsilon}_m$ and $\varepsilon \to \varepsilon_f$. With the SiC_f/Al_2O_3 material, the initially-smooth decay in creep rate with increasing strain [Fig. 4(b)] coincides with the general formation of matrix cracks throughout the testpiece gauge lengths (Figs. 11 and 13). As creep proceeds, a small strain burst is caused by the opening of a larger crack formed by complete penetration of a fibre bundle. The frequency of bundle penetration increases as creep continues, so the magnitude of the serrations on the $\dot{\varepsilon}/\varepsilon$ curves also increases. With the SiC_f/SiC samples, a dominant crack forms early in the creep life, penetrating rapidly through successive longitudinal bundles, so the $\dot{\varepsilon}/\varepsilon$ curves are serrated almost from the start of the tests [Fig. 4(a)]. Even so, as the fibre bundles fail progressively during creep of both CFCCs, the strain contributions from crack opening and stress transfer to unbroken fibre bundles are not sufficient to cause a sustained increase in overall creep rate until just before fracture. Then, as the proportion of the fracture surfaces occupied by near-planar cracks increases with decreasing stress, so that fewer unbroken bundles are supporting the creep loads as $\varepsilon \to \varepsilon_f$, a short period of rapid tertiary acceleration becomes more apparent with increasing test duration (Fig. 4).

With the SiC_f/SiC samples, the formation of a dominant crack results in a high stress concentration on the unbroken fibre bundles [Fig. 12(a)]. However, the stress concentrations are lower on the unbroken bundles distributed across the crack plane when failure occurs by link-up of cracks growing throughout the SiC_f/Al_2O_3 specimens [Fig. 12(b)]. Hence, the pull-out area/cross section ratios on the fracture surfaces range only from ~40 to 20% with the SiC_f/Al_2O_3 samples, compared with ~75 to 25% for the SiC_f/SiC testpieces over similar stress ranges. As the ductility increases with decreasing stress for the SiC_f/Al_2O_3 composite, large cracks can therefore form without causing immediate failure, indicating the potential for development of CFCCs combining crack tolerance, low density and high strength for applications involving long-term creep exposure in air at elevated temperatures.

4. Conclusions

Many features of the deformation and damage processes occurring during tensile creep in air at 1300°C are similar for 0/90° woven SiC_f/SiC and SiC_f/Al_2O_3 composites.

The longitudinal fibres control the rates of creep strain accumulation and the accompanying formation

of cracks in the weak brittle matrices. As the developing cracks penetrate into the longitudinal fibre bundles, crack growth rates are limited by crack-bridging fibres, but fibre failure is promoted by oxygen penetration. Creep fracture then takes place when the area of the developing cracks attain the critical fraction of the test-piece cross-section required for sudden failure by fibre pull-out.

Both CFCCs exhibit continuously-decaying creep curves with negligible tertiary stages, so that $\dot{\varepsilon} \rightarrow \dot{\varepsilon}_m$ and $t \rightarrow t_f$ as $\varepsilon \rightarrow \varepsilon_f$. However, low ε_f values ($\sim$0.002) were recorded in all tests carried out for the SiC_f/SiC material, whereas ε_f increased from $\sim$0.002 to $\sim$0.03 as the test duration increased towards $\sim$2500 h for the SiC_f/Al_2O_3 composite. While measurements of the initial creep rates indicate that the creep resistance of the SiC_f/Al_2O_3 is slightly superior to that of the SiC_f/SiC material, the dependences of $\dot{\varepsilon}_m$ and t_f on ε_f result in significantly lower minimum creep rates and much longer rupture lives being observed for the alumina–matrix samples.

With the SiC_f/SiC composite, low-ductility fracture is caused by a dominant crack, nucleated at macropores, growing rapidly by direct ingress of oxygen along the crack plane. In contrast, cracks form extensively throughout the SiC_f/Al_2O_3 testpieces, but crack growth rates are reduced by the double BN/SiC coatings on the Nicalon™ fibres and/or by low rates of indirect oxygen penetration through the micro-cracked alumina matrix. Low crack growth rates defer fracture to longer times and higher strains, so that ε_f increases as the crack area/cross-section ratio required to cause failure increases with decreasing stress. Hence, long cracks can develop without causing immediate failure of the SiC_f/Al_2O_3 composite during long-term creep exposure, illustrating that crack tolerance can be combined with impressive creep and creep fracture resistance for high-temperature engineering applications.

Acknowledgements

The provision of a post-doctoral research fellowship for Dr. Carreño under the EC Human Capital and Mobility Programme (Contract No. ERBCHBGCT 9330303) and the support received through the British Council UK/Spain research collaboration initiative are gratefully acknowledged. The authors also wish to thank Rolls-Royce plc for financial support and materials supplies.

References

1. Prewo, K. M., *J. Mat. Sci.*, 1986, **21**, 3590.
2. Brennan, J. J., *Mat. Sci. Res.*, 1986, **20**, 546.
3. Evans, A. G. and Marshall, B. D., *Acta Metall.*, 1989, **37**, 2657.
4. Abbé, F. and Chermant, J.-L. In *Fourth Inter. Conf. on Creep and Fracture of Engineering Materials and Structures*, ed. B. Wilshire and R. W. Evans. The Institute of Metals, London, 1990, p. 439.
5. Holmes, J. W., *J. Mat. Sci.*, 1991, **26**, 1808.
6. Kervadec, D. and Chermant, J.-L. In *Proc. Fifth Inter. Conf. on Creep and Fracture of Engineering Materials and Structures*, ed. B. Wilshire and R. W. Evans. The Institute of Materials, London, 1993, p. 371.
7. Henager Jr., C. H. and Jones, R. H., *Mat. Sci. Eng*, 1993, **A166**, 211.
8. Chermant, J.-L., *Silicates Industriels*, 1995, **60**, 261.
9. Evans, A. G. and Weber, C., *Mat. Sci. Eng*, 1996, **A208**, 1.
10. Zhu, S., Mizuno, M., Kagawa, Y., Cao, J., Nagano, Y. and Kaya, H., *Mat. Sci. Eng*, 1997, **A225**, 69.
11. Rospars, C., Chermant, J.-L. and Ladevéze, P., *Mat. Sci. Eng*, 1998, **A250**, 264.
12. Wilshire, B., Carreño, F. and Percival, M. J. L., *Scripta Materialia*, 1998, **39**, 729.
13. Newkirk, M. S., Urquhart, A. W., Zwicker, H. R. and Breval, E., *J. Mat. Res.*, 1986, **1**, 81.
14. Newkirk, M. S., Lesher, H. D., White, D. R., Kennedy, C. R., Urquhart, A. W. and Clear, T. D., *Ceram. Eng Sci. Proc.*, 1987, **8**, 879.
15. Wilshire, B. and Jiang, H., *Brit. Ceram. Trans.*, 1994, **93**, 213.
16. O'Meara, C., Suihkonen, T., Hansson, T. and Warren, R., *Mat. Sci. Eng*, 1996, **A209**, 251.
17. Simon, G. and Bunsell, A. R., *J. Mat. Sci.*, 1984, **19**, 3670.
18. Zhu, S., Mizuno, M., Cao, J. and Kagawa, Y. In *Creep Behaviour of Advanced Materials for the 21st Century*, ed. R. S. Mishra, A. K. Mukherjee and K. L. Murty. TMS, PA 1999, p. 379.
19. Carter Jr., C. H. and Davis, R. F., *J. Am. Ceram. Soc.*, 1984, **67**, 732.
20. de Arellano-López, A. R., Cumbrera, F. L., Domínguez-Rodríguez, A., Goretta, K. C. and Routbort, J. L., *J. Am. Ceram. Soc.*, 1990, **73**, 1297.
21. Lin, H. T. and Becher, P. F., *J. Am. Ceram. Soc.*, 1991, **74**, 1886.
22. Nutt, S. R. and Lipetzky, P., *Mat. Sci. Eng*, 1993, **A166**, 199.
23. Cao, H. C., Bischoff, E., Shaizero, O., Rühle, M., Evans, A. G., Marshall, D. B. and Brennan, J. J., *J. Am. Ceram. Soc.*, 1990, **73**, 1691.
24. Heredia, F. E., Evans, A. G. and Andersson, C. A., *J. Am. Ceram. Soc.*, 1995, **78**, 2790.
25. Conway, J. B., *Numerical Methods for Creep and Rupture Analyses*. Gordon and Breach, New York, 1967.
26. Garofalo, F., *Fundamentals of Creep and Creep Rupture in Metals*. MacMillan, New York, 1965.
27. Evans, R. W., Scharning, P. J. and Wilshire, B. In *Creep Behaviour of Crystalline Solids*, ed. B. Wilshire and R. W. Evans. Pineridge Press, Swansea, 1985, p. 201.
28. Evans, R. W. and Wilshire, B., *Creep of Metals and Alloys*. The Institute of Metals, London, 1985.
29. Evans, W. J. and Wilshire, B., *Trans. AIME.*, 1968, **242**, 1303.
30. Birch, J. M. and Wilshire, B, *J. Mat. Sci.*, 1974, **9**, 871.